

# Joint Beamforming and PD Orientation Design for Mobile Visible Light Communications

Shuai Ma, Jing Wang, Chun Du, Hang Li, *Member, IEEE*, Xiaodong Liu,  
Yulong Wu, Naofal Al-Dhahir, *Fellow, IEEE* and Shiyin Li

## Abstract

In this paper, we propose joint beamforming and photo-detector (PD) orientation (BO) optimization schemes for mobile visible light communication (VLC) with the orientation adjustable receiver (OAR). Since VLC is sensitive to line-of-sight propagation, we first establish the OAR model and the human body blockage model for mobile VLC user equipment (UE). To guarantee the quality of service (QoS) of mobile VLC, we jointly optimize BO with minimal UE the power consumption for both fixed and random UE orientation cases. For the fixed UE orientation case, since the transmit beamforming and the PD orientation are mutually coupled, the joint BO optimization problem is nonconvex and intractable. To address this challenge, we propose an alternating optimization algorithm to obtain the transmit beamforming and the PD orientation. For the random UE orientation case, we further propose a robust alternating BO optimization algorithm to ensure the worst-case QoS requirement of the mobile UE. Finally, the performance of joint BO optimization design schemes are evaluated for mobile VLC through numerical experiments.

## Index Terms

Mobile visible light communication, Orientation adjustable receiver, Beamforming design.

## I. INTRODUCTION

Visible light communication (VLC), which integrates communications and illuminations, has recently attracted increasing attention as a promising indoor wireless technology for the beyond fifth-generation (B5G) networks [1]–[3]. By using widely deployed light emitting diodes (LEDs) as transmitter antennas, VLC has many advantages, including being license free, huge bandwidth

S. Ma, J. Wang, Chun Du, and S. Li are with the School of Information and Control Engineering, China University of Mining and Technology, Xuzhou, 221116, China. (e-mail: {mashuai001, ts19060135p31, Chun Du, lishiyin}@cumt.edu.cn).

(380-780 THz), high transmission rate, and high energy efficiency. Thus, VLC can significantly alleviate the spectrum congestion of conventional radio-frequency (RF) communications [4]. However, due to the inherent short wavelength characteristics of the visible light, VLC is more susceptible to blockages than RF communications, resulting in severe communication rate drop leading to outage [5], [6].

To reduce the probability of being obstructed and improve receiver signal-to-noise ratio (SNR), there are generally two types of adjustable VLC receivers, i.e., angle diversity receiver (ADR) [7]–[9] and orientation adjustable receiver (OAR) [10]–[20]. Specifically, ADR employs multiple photo-detectors (PDs) with different orientations to achieve multiplexing gain [7], while OAR can flexibly adjust the orientations of PDs to align with the direction of incident VLC signals. Compared with ADR's reliance on multiple PDs, OAR can be implemented even with a single PD. Therefore, OAR is more flexible. Generally, there are two approaches to realize OAR, i.e., mechanical control steering [10]–[14], and metasurfaces steering [15]–[20]. On one hand, the mechanical control steering manipulates the orientations of PDs by employing mechanical machine control. Based on this setup, a slow beam steering scheme [10] was proposed to maximize the rates of the VLC system by utilizing piezoelectric actuators. A controlled field of view (FOV) was exploited to improve handover performance [11], support device mobility [12], and mitigate interference [13]. In [14], a linear zero-forcing precoding scheme was developed for multiuser multiple-input single-output VLC systems, where each user could select a specific receiving orientation angle from a set of possible orientations. On the other hand, the metasurfaces steering explores the principle of the metasurfaces infrastructure and the physico-chemical characteristics [15]–[20], to realize focal length tuning [15] (e.g., defocus), astigmatism and shift. Such metasurface-based steering scheme has shorter response time than the mechanical control steering scheme, and thus has attracted increasing research attention. In [16], an autofocusing airy beam steering scheme was designed to flexibly adjust the focal length of visible light. In [18], liquid-crystal (LC) -based optical phased arrays were developed for visible-light beam steering. In [19], two types of intelligent meta-elements to steer the incident light beam, i.e., a meta-lens with electrically stretchable artificial muscles and a LC-based re-configurable intelligent surface (RIS) infrastructure with electronically adjustable refractive index, were presented for VLC systems. The authors in [20] further proposed an LC-based RIS to enhance the VLC signal detection capacity and transmission range. Given the existing related works [15]–[20], the performance of the metasurfaces steering for VLC is still

in the preliminary stage.

Note that most of the exiting works [11]–[13] assume that the PD’s orientation can be perfectly aligned with the direction of the incident light. However, for more general practical mobile VLC scenarios, the user equipment (UE) may move and rotate. Thus, the PD’s orientation of the mobile UE is changing and may not always accurately be aligned with the direction of the incident light, which will lead to the deterioration of VLC performance. Motivated by the above discussion, we focus on jointly designing the beamforming and PD orientation (BO) for mobile VLC with fixed and random UE orientation, respectively. Note that the proposed joint BO scheme can be applied for both mechanical control steering and metasurfaces steering schemes. The main contributions of this paper are summarized as follows:

- To describe the mobile VLC, we first establish the mobile UE orientation rotation model. Then, we characterize the channel blockage model of mobile UE, which includes specific models for OAR and human blockage. Moreover, we analyze two types of OAR physical structures for mobile UE, i.e., mechanical control receiver and tunable LC receiver.
- Furthermore, for the fixed UE orientation, we jointly optimize the transmit beamforming vector and the PD orientation vector to minimize the total transmit power of LEDs, while satisfying the minimal rate requirement. Since the transmit beamforming and the PD orientation are mutually coupled, the joint BO optimization problem is non-convex and intractable. To tackle the complicated joint optimization problem, we decompose it into two sub-problems, i.e., the beamforming subproblem and PD orientation subproblem. Then, we transform both beamforming subproblem and PD orientation subproblem to convex problems, and propose an alternating optimization (AO) algorithm to iteratively solve the transmit beamformer and the PD orientation.
- Moreover, for the random UE orientation, we describe the random UE orientation model, and derive the corresponding imperfect channel state information (CSI) model. Based on the imperfect CSI model, we further investigate robust joint BO optimization problem to minimize the transmit power subject to the worst-case quality of service (QoS) requirement, which is NP-hard. To make the over-complicated problem tractable, we propose to break down the robust joint BO optimization problem into robust beamforming subproblem and PD orientation subproblem. For a given UE orientation, we effectively optimize robust beamforming by utilizing the semidefinite relaxation (SDR) method. With a fixed robust beamformer, the PD orientation subproblem is a non-linear non-smooth problem, and we

provide an alternating optimization and projection method.

The rest of this paper is organized as follows. Section II describes the OAR-based system model. In Section III, we present the joint BO scheme for the fixed UE orientation case. The case of random UE orientation is discussed in Section IV. The simulation and numerical results are provided in Section V. Finally, the paper is concluded in Section VI. Table I presents the means of the key notations in this paper.

TABLE I: Summary of Key Notations

Notation	Description
$\theta, \omega$	Elevation and azimuth angle of PD orientation vector
$\mathbf{g}(\theta, \omega)$	Channel gain function of $\theta, \omega$
$\hat{\mathbf{n}}_{\text{UE}}$	UE orientation vector in the Earth coordinate
$\mathbf{n}_{\text{UE}}$	UE orientation vector in the UE coordinate
$\mathbf{n}_{\text{OAR}}$	PD orientation vector in the UE coordinate
$u_i$	Indicator parameter of blockage model
$R(\theta, \omega, \mathbf{p})$	Achievable rate of fixed UE orientation
$R_{\text{mob}}(\mathbf{n}_{\text{OAR}}, \mathbf{p})$	Achievable rate of random UE orientation
$\mathbf{e}_i$	Unit vector with the $i$ -th element equal to 1

*Notations:* Boldfaced lowercase and uppercase letters represent vectors and matrices, respectively. The transpose, Frobenius norm, Hadamard-product, trace of a matrix and expectation are denoted as  $(\cdot)^T$ ,  $\|\cdot\|$ ,  $\odot$ ,  $\text{Tr}(\cdot)$ , and  $\mathbb{E}\{\cdot\}$ , respectively.  $\mathcal{N} \triangleq \{1, 2, \dots, N\}$ .

## II. MOBILE VLC SYSTEM MODEL

Consider a downlink mobile VLC system, where a lamp with  $N$  LEDs can transmit information to a mobile UE with single PD. Let  $s$  denote the transmitted signal and it follows the amplitude constraint, i.e.,  $|s| \leq A$ . Meanwhile,  $\mathbb{E}\{s\} = 0$  and  $\mathbb{E}\{s^2\} = \varepsilon$ . Moreover, let  $\mathbf{p} = [\sqrt{p_1}, \dots, \sqrt{p_N}]^T \in \mathbb{R}^N$  denote the beamforming vector, where  $p_i$  is the power gain for the  $i$ th LED. Thus, the transmitted signal  $\mathbf{x}$  can be written as

$$\mathbf{x} = \mathbf{p}s + I_{\text{DC}}\mathbf{1}_N, \quad (1)$$

where  $I_{\text{DC}} \geq 0$  is the direct current (DC) bias at each LED,  $\mathbf{1}_N$  denotes a  $N \times 1$  vector with all element equal to 1. To ensure the non-negativity of the transmitted signal, the power gain  $p_i$  of the  $i$ th LED satisfies

$$\sqrt{p_i}A \leq I_{\text{DC}}, \forall i \in \mathcal{N}. \quad (2)$$

At the UE side, the received signal is from both the line-of-sight (LOS) channel and reflection channel. In many scenarios, the gains of reflection channels are much lower than those of the LOS channels [21], [22]. In this paper, we only consider cases of LOS channel dominating the transmission, i.e., the NLOS transition coefficient is less than 0.5. Let  $\mathbf{g}(\theta, \omega) = [g_1(\theta, \omega), \dots, g_N(\theta, \omega)]^T$  denote the channel gain vector, where  $g_i(\theta, \omega)$  is the channel gain between the  $i$ th LED and the UE. Note that the channel gain vector  $\mathbf{g}(\theta, \omega)$  is a function of  $\theta, \omega$ , which vary with OAR's orientation. We will specify the channel gain vector in the following subsections. By using the above definitions, the received signal  $y$  at the UE is given by

$$y = \mathbf{g}(\theta, \omega)^T \mathbf{x} + z, \quad (3)$$

where  $z$  is the received real Gaussian noise with mean zero and variance  $\sigma^2$ .

#### A. UE Coordination System

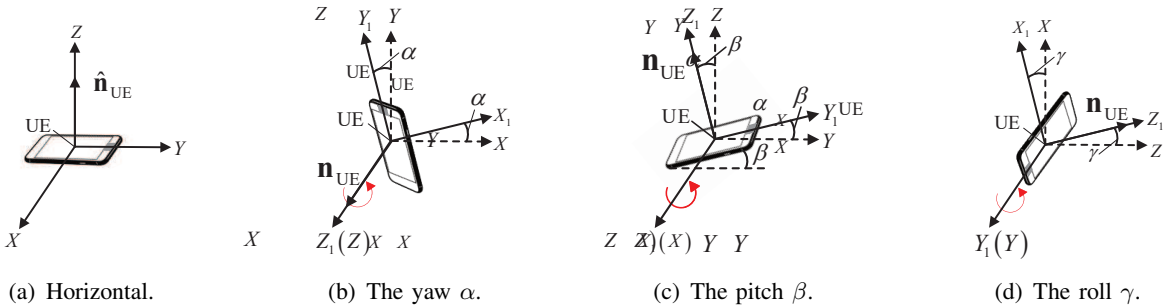


Fig. 1: The UE coordination system and its rotation.

To quantify the UE orientation, we first introduce the UE coordination system, as shown in Fig. 1, where  $\mathbf{n}_{\text{UE}}$  denotes the orientation of the UE. When it is placed as shown in Fig. 1 (a), its direction is aligned with the Z-axis. Let  $\hat{\mathbf{n}}_{\text{UE}}$  denote the orientation vector of UE in the Earth coordinate  $X$ - $Y$ - $Z$  (in which the  $X$ - $Y$  plane is the horizontal plane). The UE rotation is usually defined by the yaw, pitch, and roll. Specifically, as shown in Fig. 1 (b)-(d), the yaw is the positive rotation around the Z-axis with an angle of  $\alpha$ , pitch is around the X-axis with an angle of  $\beta$ , and roll is around the Y-axis with an angle of  $\gamma$ .

According to Euler's rotation theorem [23], the rotation can be uniquely expressed by three elements  $\mathbf{R}_\alpha, \mathbf{R}_\beta, \mathbf{R}_\gamma$ , which are the yaw, pitch and roll matrices corresponding to  $\alpha, \beta,$  and  $\gamma$ , respectively. Specifically, the expressions for the yaw, pitch and roll matrices are given as

$$\mathbf{R}_\alpha = \begin{bmatrix} \cos \alpha & -\sin \alpha & 0 \\ \sin \alpha & \cos \alpha & 0 \\ 0 & 0 & 1 \end{bmatrix}, \mathbf{R}_\beta = \begin{bmatrix} 1 & 0 & 0 \\ 0 & \cos \beta & -\sin \beta \\ 0 & \sin \beta & \cos \beta \end{bmatrix}, \mathbf{R}_\gamma = \begin{bmatrix} \cos \gamma & 0 & \sin \gamma \\ 0 & 1 & 0 \\ -\sin \gamma & 0 & \cos \gamma \end{bmatrix}. \quad (4)$$

Let  $\mathbf{R} = \mathbf{R}_\alpha \mathbf{R}_\beta \mathbf{R}_\gamma$  denote the rotated matrix. After the rotation, we obtain the UE coordinate system  $X_1-Y_1-Z_1$ . To coincide with the UE coordinate system, we assume that the initial corresponding UE normal vector is  $\mathbf{n}_{\text{UE}} = [0, 0, 1]^T$ . It is clear that  $\mathbf{n}_{\text{UE}} = \mathbf{R}^{-1} \hat{\mathbf{n}}_{\text{UE}}$  based on the coordinate transformation theory.

### B. OAR Model

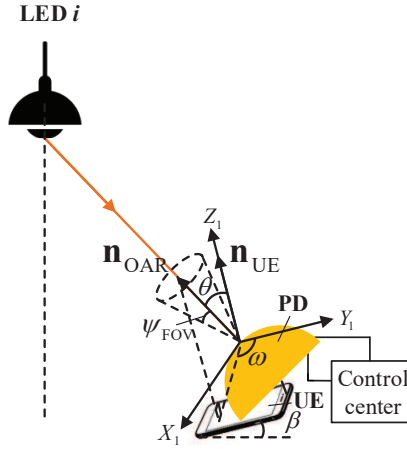


Fig. 2: The directional geometry of OAR.

The alignment of the PD and the LED can be mathematically described via the OAR model. Since the PD is adjustable, its orientation can be different from the UE orientation. Let  $\mathbf{n}_{\text{OAR}}(\theta, \omega)$  denote the normalized PD orientation vector in the UE coordinate  $X_1-Y_1-Z_1$ , where the  $X_1-Y_1$  plane is parallel to the UE plane, and the  $Z_1$  axis is perpendicular to the UE plane. As shown in Fig. 2, the orientation vector  $\mathbf{n}_{\text{OAR}}(\theta, \omega)$  can be expressed as

$$\mathbf{n}_{\text{OAR}}(\theta, \omega) = [\sin \theta \cos \omega, \sin \theta \sin \omega, \cos \theta]^T, \quad (5)$$

where  $\theta$  is the elevation angle between  $\mathbf{n}_{\text{OAR}}(\theta, \omega)$  and the  $Z_1$  axis, and  $\omega$  is the azimuth angle between the projection of  $\mathbf{n}_{\text{OAR}}(\theta, \omega)$  in the  $X_1$ - $Y_1$  plane and the  $Y_1$  axis.

By controlling  $\theta$  and  $\omega$ , PD can be aligned with the LED as much as possible. Generally, physical schemes to realize OAR are a mechanical control receiver (MCR) and a tunable liquid-crystal receiver (TLR), which are discussed next.

- **Mechanical Control Receiver:** The PD orientation is adjusted by micro electromechanical systems. More specifically, MCR can freely adjust the PD rotation by a sophisticated mechanical module, and thus the PD direction  $\mathbf{n}_{\text{OAR}}(\theta, \omega)$  can be aligned with the light incident direction to some extent. As shown in Fig. 2, the angle between the UE and the horizontal plane is  $\beta$ , and after adjusting the PD orientation by MCR, the PD orientation vector  $\mathbf{n}_{\text{OAR}}(\theta, \omega)$  can be aligned with the LED. Consequently, when the user is moving, the PD of the receiver can be aimed at the strongest incident angle of the light in real time.
- **Tunable Liquid-crystal Receiver:** A TLR can effectively manipulate the angle of incident light at the PD by using the external electrical facility [19]. Specifically, TLR is a synthesized material composed of dielectric structures and liquid-crystal cells, which are used to manipulate the light propagation in unusual ways compared to classical optical devices. The liquid-crystal cell is capable of realizing the adjustable refractive index, which exactly affects the direction and intensity of refracted light [15], [24]. As shown in Fig. 2, TLR can change its orientation  $\mathbf{n}_{\text{OAR}}(\theta, \omega)$  to steer the LED.

With orientation adjustable schemes MCR or TLR, the orientation of PDs may perfectly align with the LED when the UE orientation is fixed. However, when the UE is moving, the UE orientation may change and can be random. Thus, the orientation of PDs may not accurately and timely align with the LED, because it takes time to adjust the orientation. The fixed and random UE orientation cases will be further discussed in Sections III and IV, respectively.

### C. Blockage Model

Due to the UE mobility, the LOS link may suffer from blockage, which would significantly influence the channel power gain. In practice, the VLC is vulnerable to blocking, especially by the mobile user itself [5], [25]. As shown in Fig. 3 (a), let  $\mathbf{r}_{\text{UE}} = [x_{\text{UE}}, y_{\text{UE}}, z_{\text{UE}}]^T$  and  $\mathbf{x}_{\text{L},i} = [x_{\text{L},i}, y_{\text{L},i}, z_{\text{L},i}]^T$  denote the UE position and the  $i$ th LED, respectively. Moreover,  $\mathbf{n}_{\text{u}}$  is defined as the normal vector of the human's forward direction, and  $\mathbf{x}_{\text{b}} = [x_{\text{b}}, y_{\text{b}}, z_{\text{b}}]^T$  is defined as an intersecting point of the blocked incident light and the human body.

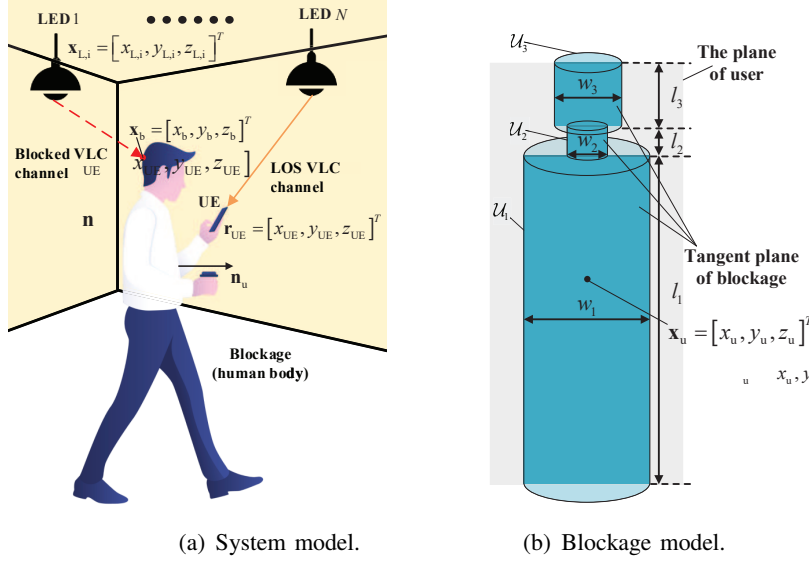


Fig. 3: The schematic of the blockage model of mobile UE.

To characterize the blockage model, we model the head, neck and body of the person as three cylinders  $\mathcal{U}_1$ ,  $\mathcal{U}_2$  and  $\mathcal{U}_3$ , respectively, as shown in Fig. 3 (b). Specifically, let  $w_i$  and  $l_i$  denote the diameter and the height of the cylinder  $\mathcal{U}_i$ , respectively, where  $i = 1, 2$  and  $3$ . Moreover, let  $\mathbf{x}_u = [x_u, y_u, z_u]^T$  denote the center of gravity position of the person. The area of  $\mathcal{U}_1$  can be expressed as

$$\mathcal{U}_1 \triangleq \left\{ \mathbf{x}_0 \left| \begin{array}{l} (x_0 - x_u)^2 + (y_0 - y_u)^2 \leq \left(\frac{w_1}{2}\right)^2, \\ 0 \leq \mathbf{x}_0^T \mathbf{e}_3 \leq l_1 \end{array} \right. \right\}, \quad (6)$$

where  $\mathbf{e}_3 \triangleq [0, 0, 1]^T$ . Similarly, the areas of  $\mathcal{U}_2$  and  $\mathcal{U}_3$  are respectively given as

$$\mathcal{U}_2 \triangleq \left\{ \mathbf{x}_0 \left| \begin{array}{l} (x_0 - x_u)^2 + (y_0 - y_u)^2 \leq \left(\frac{w_2}{2}\right)^2, \\ l_1 \leq \mathbf{x}_0^T \mathbf{e}_3 \leq (l_1 + l_2) \end{array} \right. \right\}, \quad (7)$$

$$\mathcal{U}_3 \triangleq \left\{ \mathbf{x}_0 \left| \begin{array}{l} (x_0 - x_u)^2 + (y_0 - y_u)^2 \leq \left(\frac{w_3}{2}\right)^2, \\ (l_1 + l_2) \leq \mathbf{x}_0^T \mathbf{e}_3 \leq (l_1 + l_2 + l_3) \end{array} \right. \right\}. \quad (8)$$

Since we focus on the LOS channel of the VLC link, the blockage may occur when the following two conditions happen simultaneously: the direction of the incident light points to the back of the human body, since the UE is usually held in front of the human body; and the human

body is at the LOS between the LED and the UE. These two conditions can be mathematically described as follows

**Condition I:** When the direction of the incident light points to the back of the human, the angle between the human forward direction vector  $\mathbf{n}_u$  and incident light vector  $(\mathbf{x}_{L,i} - \mathbf{r}_{UE})$  is an obtuse angle, i.e.,

$$\mathbf{n}_u^T (\mathbf{x}_{L,i} - \mathbf{r}_{UE}) \leq 0. \quad (9)$$

**Condition II:** There is an intersection point  $\mathbf{x}_b$  between the incident light line and the human body. Specifically, the line equation between the  $i$ th LED and the UE is given as

$$\frac{x_b - x_{UE}}{x_{L,i} - x_{UE}} = \frac{y_b - y_{UE}}{y_{L,i} - y_{UE}} = \frac{z_b - z_{UE}}{z_{L,i} - z_{UE}}. \quad (10)$$

Using a tangent plane of blockage as the constrained blockage plane, as shown in Fig. 1(b), which can be achieved by cutting the cylinder model. Specifically, the tangent blockage plane is given as

$$\begin{cases} \mathbf{x}_b \in \{\mathcal{U}_1 \cup \mathcal{U}_2 \cup \mathcal{U}_3\}, \\ \mathbf{n}_u^T (\mathbf{x}_b - \mathbf{x}_u) = 0. \end{cases} \quad (11)$$

Thus, we have obtained intersection point  $\mathbf{x}_b$  by jointly solving Equations (10) and (11).

Therefore, when the Conditions I and II are met simultaneously, the incident light is blocked by the human body. We use an indicator parameter  $u_i$  to describe whether the LOS link between the  $i$ th LED and UE is blocked or not, i.e.,  $u_i = 1$  means LOS link is blocked, while  $u_i = 0$  means LOS link is not blocked.

#### D. Channel Gain and Achievable Rate Expressions

According to the Lambertian model, the channel gain  $g_i$  for the  $i$ th LED can be expressed as

$$g_i = \frac{u_i(m+1)A_r}{2\pi d_i^2} \cos^m(\phi_i) \Gamma_i(\varphi_i, \psi_{\text{FOV}}) \cos(\varphi_i), \quad (12)$$

where  $\Gamma_i(\varphi_i, \psi_{\text{FOV}}) = 1$  when  $|\varphi_i| \leq \psi_{\text{FOV}}$  and otherwise  $\Gamma_i(\varphi_i, \psi_{\text{FOV}}) = 0$ . The parameter  $\psi_{\text{FOV}}$  is the field of vision (FOV) of PD,  $m = -\ln 2 / \ln(\cos(\phi_{1/2}))$  is the Lambertian index of the LED,  $\phi_{1/2}$  is the semi-angle,  $d_i$  is the distance between the  $i$ th LED and the PD,  $A_r$  is the effective area of the PD,  $\phi_i$  is the irradiance angle, and  $\varphi_i$  is the incidence angle.

Based on the OAR and the blockage models, we derive the channel gain expression as a function of the variables  $\theta, \omega$  in the UE coordinate system. Let  $\tilde{\mathbf{x}}_{L,i}$  and  $\tilde{\mathbf{r}}_{\text{UE}}$ , respectively, denote the locations of the  $i$ th LED and UE in the UE coordinate system  $X_1$ - $Y_1$ - $Z_1$ , which are given as

$$\tilde{\mathbf{x}}_{L,i} = \mathbf{R}^{-1} \mathbf{x}_{L,i}, \tilde{\mathbf{r}}_{\text{UE}} = \mathbf{R}^{-1} \mathbf{r}_{\text{UE}}. \quad (13)$$

Therefore, the terms  $\cos(\phi_i)$  and  $\cos(\varphi_i)$  in (12) can be, respectively, rewritten as

$$\cos(\phi_i) = \frac{z_{L,i} - z_{\text{UE}}}{d_i}, \quad (14a)$$

$$\cos(\varphi_i) = \frac{(\tilde{\mathbf{x}}_{L,i} - \tilde{\mathbf{r}}_{\text{UE}})^T \mathbf{n}_{\text{OAR}}(\theta, \omega)}{d_i}. \quad (14b)$$

Substituting (14) into (12), the channel gain  $g_i(\theta, \omega)$  between the  $i$ th LED and the UE can be re-expressed as

$$g_i(\theta, \omega) = \lambda_i \mathbf{d}_i^T \mathbf{n}_{\text{OAR}}(\theta, \omega) \Gamma_i(\mathbf{n}_{\text{OAR}}(\theta, \omega)), \quad (15)$$

where  $\lambda_i = \frac{u_i A_{\Gamma}(m+1)(z_{L,i} - z_{\text{UE}})^m}{2\pi d_i^{m+3}}$ ,  $\mathbf{d}_i = \tilde{\mathbf{x}}_{L,i} - \tilde{\mathbf{r}}_{\text{UE}}$  is the incident vector between the  $i$ th LED and the UE in the UE coordinate system, and  $\Gamma_i(\mathbf{n}_{\text{OAR}}(\theta, \omega))$  is the indicator function of  $\mathbf{n}_{\text{OAR}}(\theta, \omega)$  given as

$$\Gamma_i(\mathbf{n}_{\text{OAR}}(\theta, \omega)) = \begin{cases} 1, & \frac{\mathbf{d}_i^T \mathbf{n}_{\text{OAR}}(\theta, \omega)}{d_i} \geq \cos(\psi_{\text{FOV}}), \\ 0, & \text{otherwise.} \end{cases} \quad (16)$$

Since the channel capacity of VLC channels is unknown, we adopt the ABG lower bound with close-form expression [26] analyze the mobile VLC system, i.e.,

$$R(\theta, \omega, \mathbf{p}) = B \log_2 \left( 1 + \frac{|\mathbf{g}(\theta, \omega)^T \mathbf{p}|^2 e^{1+2(\alpha_0 + \gamma_0 \varepsilon)}}{2\pi B \sigma^2} \right), \quad (17)$$

where  $B$  denotes the bandwidth of the VLC system. Moreover, the parameters  $\alpha_0$ ,  $\beta_0$  and  $\gamma_0$  are determined by the inputs constraints  $|s| \leq A$ ,  $\mathbb{E}\{s\} = 0$  and  $\mathbb{E}\{s^2\} = \varepsilon$  as follows

$$T(A) - T(-A) = e^{1+\alpha_0}, \quad (18a)$$

$$\beta_0 (e^{A(\beta_0 - \gamma_0 A)} - e^{-A(\beta_0 + \gamma_0 A)} - e^{1+\alpha_0}) = 0, \quad (18b)$$

$$e^{A(\beta_0 - \gamma_0 A)} ((\beta_0 - 2\gamma_0 A) e^{-2A\beta_0} - \beta_0 - 2\gamma_0 A) + (\beta_0^2 + 2\gamma_0) e^{1+\alpha_0} = 4\gamma_0^2 \varepsilon e^{1+\alpha_0}, \quad (18c)$$

where  $T(x) \triangleq \frac{\sqrt{\pi}}{2\sqrt{\gamma_0}} e^{\frac{\beta_0^2}{4\gamma_0}} \operatorname{erf}\left(\frac{\beta_0 + 2\gamma_0 x}{2\sqrt{\gamma_0}}\right)$ .

### III. JOINT BO SCHEME DESIGN FOR FIXED UE ORIENTATION

To begin with, we consider the case of fixed UE orientation, i.e., the normal orientation vector  $\mathbf{n}_{\text{UE}}$  of UE is fixed with certain angles, and the orientations of PD can be adjusted to align with the LED. Based on the OAR's orientation analysis in the previous section, we further jointly optimize BO, i.e., the elevation angle  $\theta$  and azimuth angle  $\omega$ , and beamformer  $\mathbf{p}$ , to minimize the total transmit power of LEDs, while satisfying both the orientation angle and rate constraints. Mathematically, the joint beamforming and orientation optimization problem can be formulated as

$$\min_{\theta, \omega, \mathbf{p}} \varepsilon \|\mathbf{p}\|^2 \quad (19a)$$

$$\text{s.t. } R(\theta, \omega, \mathbf{p}) \geq \bar{R}, \quad (19b)$$

$$0 \leq \theta \leq \bar{\theta}, \quad (19c)$$

$$-\pi \leq \omega \leq \pi, \quad (19d)$$

$$\sqrt{p_i} A \leq I_{\text{DC}}, \forall i \in \mathcal{N}, \quad (19e)$$

where  $\bar{R}$  is the minimum rate requirement of the UE, and  $\bar{\theta} \in (0, \frac{\pi}{2}]$  is the elevation angle  $\theta$  threshold. Since the elevation angle  $\theta$  and azimuth angle  $\omega$  are coupled in (19b), problem (19) is non-convex and computationally intractable. To address this challenge, we first reformulate problem (19) into a more concise form by merging the optimization variables. Recall that  $\|\mathbf{n}_{\text{OAR}}\|^2 = 1$ , since the orientation vector  $\mathbf{n}_{\text{OAR}}(\theta, \omega)$  is a normal vector. Given that  $\cos\theta$  is a monotonically decreasing function for  $0 \leq \theta \leq \bar{\theta}$  and  $\sin\omega$  is a monotonically increasing function for  $-\pi \leq \omega \leq \pi$ ,  $\mathbf{n}_{\text{OAR}}(\theta, \omega)$  is a one-to-one mapping of variables  $(\theta, \omega)$ . Then, since  $0 \leq \theta \leq \bar{\theta}$ , we have  $\cos^2\bar{\theta} \leq \cos\theta \leq 1$ . Thus, by projecting the orientation vector  $\mathbf{n}_{\text{OAR}}(\theta, \omega)$  into the  $X_1$ - $Y_1$  plane, we have

$$(\sin\theta \cos\omega)^2 + (\sin\theta \sin\omega)^2 \leq \sin^2\bar{\theta}. \quad (20)$$

Furthermore, constraints (19c) and (19d) can be equivalently rewritten as

$$\|(\mathbf{e}_1 + \mathbf{e}_2) \odot \mathbf{n}_{\text{OAR}}\|^2 \leq \sin^2\bar{\theta}, \quad (21a)$$

$$\cos \bar{\theta} \leq \mathbf{n}_{\text{OAR}}^T \mathbf{e}_3 \leq 1, \quad (21b)$$

where  $\mathbf{e}_i$  is a unit vector with the  $i$ -th element equal to 1,  $i = 1, 2$  and 3. Therefore, based on the orientation vector  $\mathbf{n}_{\text{OAR}}$ , problem (19) can be equivalently reformulated as

$$\min_{\mathbf{n}_{\text{OAR}}, \mathbf{p}} \varepsilon \|\mathbf{p}\|^2 \quad (22a)$$

$$\text{s.t. } B \log_2 \left( 1 + \frac{|\mathbf{g}(\mathbf{n}_{\text{OAR}})^T \mathbf{p}|^2 e^{1+2(\alpha_0 + \gamma_0 \varepsilon_0)}}{2\pi B \sigma^2} \right) \geq \bar{R}, \quad (22b)$$

$$\|(\mathbf{e}_1 + \mathbf{e}_2) \odot \mathbf{n}_{\text{OAR}}\|^2 \leq \sin^2 \bar{\theta}, \quad (22c)$$

$$\cos \bar{\theta} \leq \mathbf{n}_{\text{OAR}}^T \mathbf{e}_3 \leq 1, \quad (22d)$$

$$\|\mathbf{n}_{\text{OAR}}\|^2 = 1, \quad (22e)$$

$$\sqrt{p_i} A \leq I_{\text{DC}}, \forall i \in \mathcal{N}. \quad (22f)$$

Note that, due to the coupling of the beamforming vector  $\mathbf{p}$  and the orientation vector  $\mathbf{n}_{\text{OAR}}$ , problem (22) is still non-convex and intractable. To make this complicated problem tractable, we first decouple the beamforming vector  $\mathbf{p}$  and the orientation vector  $\mathbf{n}_{\text{OAR}}$  by decomposing problem (22) into two sub-problems, i.e., a beamforming design subproblem and a PD orientation subproblem. Specifically, we propose an alternating optimization and projection algorithm to handle problem (22), in which the transmit beamforming vector  $\mathbf{p}$  and the PD orientation vector  $\mathbf{n}_{\text{OAR}}$  are alternately optimized.

### A. Beamforming Design Subproblem

For a given PD orientation  $\mathbf{n}_{\text{OAR}}$ , the beamforming design subproblem of (19) is given as

$$\min_{\mathbf{p}} \varepsilon \|\mathbf{p}\|^2 \quad (23a)$$

$$\text{s.t. } B \log_2 \left( 1 + \frac{|\mathbf{g}(\mathbf{n}_{\text{OAR}})^T \mathbf{p}|^2 e^{1+2(\alpha_0 + \gamma_0 \varepsilon_0)}}{2\pi B \sigma^2} \right) \geq \bar{R}, \quad (23b)$$

$$\sqrt{p_i} A \leq I_{\text{DC}}, \forall i \in \mathcal{N}, \quad (23c)$$

which is also non-convex. To address the non-convexity issue, we apply the SDR technique to relax problem (23). Specifically, by using the following relationship

$$\mathbf{P} = \mathbf{p}\mathbf{p}^T \Leftrightarrow \text{rank}(\mathbf{P}) = 1, \mathbf{P} \succeq \mathbf{0}, \quad (24)$$

and neglecting the non-convex rank-1 constraint, problem (23) can be reformulated as

$$\min_{\mathbf{P}} \varepsilon \text{Tr}(\mathbf{P}) \quad (25a)$$

$$\text{s.t. } \text{Tr}(\mathbf{P}\mathbf{g}(\mathbf{n}_{\text{OAR}})\mathbf{g}(\mathbf{n}_{\text{OAR}})^T) \geq c_1, \quad (25b)$$

$$\text{Tr}(\mathbf{P}\mathbf{e}_i\mathbf{e}_i^T) \leq \frac{I_{\text{DC}}^2}{A}, \forall i \in \mathcal{N}, \quad (25c)$$

$$\mathbf{P} \succeq \mathbf{0}, \quad (25d)$$

where  $c_1 = \left(2^{\frac{\bar{R}}{B}} - 1\right) \frac{2\pi B\sigma^2}{e^{1+2(\alpha_0+\gamma_0\varepsilon)}}$ . Problem (25) is a convex semidefinite program (SDP), and the optimal beamforming vector  $\mathbf{P}_o$  can be obtained by interior-point algorithms [27] [28]. The computation complexity of (25) is  $\mathcal{O}((N+2)^4 N^{1/2} \log(1/\zeta_1))$ , where  $\zeta_1 > 0$  is the solution accuracy [29]. Note that if  $\text{rank}(\mathbf{P}_o) = 1$ , the optimal beamforming vector  $\mathbf{p}_o$  of problem (23) can be obtained by eigenvalue decomposition. Due to SDR, the case  $\text{rank}(\mathbf{P}_o) > 1$  may also occur. In this case, we can use the Gaussian randomization procedure to generate a high-quality feasible beamformer vector  $\mathbf{p}_o$  [29].

### B. PD Orientation Subproblem

For a given beamformer vector  $\mathbf{p}_o$ , the PD orientation optimization subproblem is given by

$$\min_{\mathbf{n}_{\text{OAR}}} \varepsilon \|\mathbf{p}_o\|^2 \quad (26a)$$

$$\text{s.t. } B \log_2 \left( 1 + \frac{|\mathbf{g}(\mathbf{n}_{\text{OAR}})^T \mathbf{p}_o|^2 e^{1+2(\alpha_0+\gamma_0\varepsilon)}}{2\pi B\sigma^2} \right) \geq \bar{R}, \quad (26b)$$

$$\|(\mathbf{e}_1 + \mathbf{e}_2) \odot \mathbf{n}_{\text{OAR}}\|^2 \leq \sin^2 \bar{\theta}, \quad (26c)$$

$$\cos \bar{\theta} \leq \mathbf{n}_{\text{OAR}}^T \mathbf{e}_3 \leq 1, \quad (26d)$$

$$\|\mathbf{n}_{\text{OAR}}\|^2 = 1. \quad (26e)$$

Note that problem (26) is an optimization problem of finding feasible solutions satisfying both the orientation constraints and the minimum rate constraint. However, there are many feasible

solutions satisfying constraints (26b),(26c) and (26d). Moreover, the objective function (26a) decreases with the power of beamforming vector  $\|\mathbf{p}_o\|^2$ , and is independent of  $\mathbf{n}_{\text{OAR}}$ . Thus, we optimize the orientation vector  $\mathbf{n}_{\text{OAR}}$  to minimize the transmission power with the maximum  $\mathbf{g}(\mathbf{n}_{\text{OAR}})^T \mathbf{p}_o$ . Then, the PD orientation subproblem (26) can be reformulated as

$$\begin{aligned} \max_{\mathbf{n}_{\text{OAR}}} \quad & \mathbf{g}(\mathbf{n}_{\text{OAR}})^T \mathbf{p}_o \\ \text{s.t.} \quad & (26\text{b}), (26\text{c}), (26\text{d}), (26\text{e}). \end{aligned} \quad (27)$$

To address subproblem (27), the objective function of (27) with PD orientation vector  $\mathbf{n}_{\text{OAR}}$  can be reformulated as

$$\mathbf{g}(\mathbf{n}_{\text{OAR}})^T \mathbf{p}_o = \sum_{i=1}^N \lambda_i \sqrt{p_i} \mathbf{d}_i^T \mathbf{n}_{\text{OAR}} \Gamma_i(\mathbf{n}_{\text{OAR}}). \quad (28)$$

Based on the expansion expression (28), constraint (26b) can be rewritten as

$$\sum_{i=1}^N \lambda_i \sqrt{p_i} \mathbf{d}_i^T \mathbf{n}_{\text{OAR}} \Gamma_i(\mathbf{n}_{\text{OAR}}) \geq c_2, \quad (29)$$

where  $c_2 = \sqrt{\left(2^{\frac{\bar{R}}{B}} - 1\right) \frac{2\pi B \sigma^2}{e^{1+2(\alpha_0+\gamma_0\epsilon_0)}}}$ . Furthermore, we relax the equality constraint  $\|\mathbf{n}_{\text{OAR}}\|^2 = 1$  as  $\|\mathbf{n}_{\text{OAR}}\|^2 \leq 1$ . Therefore, the PD orientation subproblem (27) can be reformulated as

$$\max_{\mathbf{n}_{\text{OAR}}} \sum_{i=1}^N \lambda_i \sqrt{p_i} \mathbf{d}_i^T \mathbf{n}_{\text{OAR}} \Gamma_i(\mathbf{n}_{\text{OAR}}) \quad (30\text{a})$$

$$\text{s.t.} \quad \sum_{i=1}^N \lambda_i \sqrt{p_i} \mathbf{d}_i^T \mathbf{n}_{\text{OAR}} \Gamma_i(\mathbf{n}_{\text{OAR}}) \geq c_2, \quad (30\text{b})$$

$$\|(\mathbf{e}_1 + \mathbf{e}_2) \odot \mathbf{n}_{\text{OAR}}\|^2 \leq \sin^2 \bar{\theta}, \quad (30\text{c})$$

$$\cos \bar{\theta} \leq \mathbf{n}_{\text{OAR}}^T \mathbf{e}_3 \leq 1, \quad (30\text{d})$$

$$\|\mathbf{n}_{\text{OAR}}\|^2 \leq 1. \quad (30\text{e})$$

Due to the integer and indicator function  $\Gamma_i(\mathbf{n}_{\text{OAR}})$  in both objective function (30a) and constraint (30b), problem (30) is a non-linear non-smooth problem [30], which is hard to solve. To overcome the NP-hard challenging issue, we propose an iterative optimization and projection method to handle problem (30). To be more specific, during the  $k$ th iteration, we relax this

problem (30) as follows

$$\max_{\mathbf{n}_{\text{OAR}}} \sum_{j \in \mathcal{M}} \lambda_j \sqrt{p_j} \mathbf{d}_j^T \mathbf{n}_{\text{OAR}} \quad (31a)$$

$$\text{s.t.} \quad \sum_{j \in \mathcal{M}} \lambda_j \sqrt{p_j} \mathbf{d}_j^T \mathbf{n}_{\text{OAR}} \geq c_2, \quad (31b)$$

$$(30c), (30d), (30e),$$

where  $\mathcal{M} \triangleq \left\{ \forall j \in \mathcal{N} \mid \Gamma_j \left( \tilde{\mathbf{n}}_{\text{OAR}}^{[m]} \right) \neq 0 \right\}$  describes the LEDs set. Then, by applying the standard interior-point algorithm [27], problem (31) can be efficiently solved and the solution  $\tilde{\mathbf{n}}_{\text{OAR}}^{[m]}$  can be obtained. Then, the LEDs set  $\mathcal{M}$  is updated. Furthermore, we decide the value of the indicator function  $\Gamma_i \left( \tilde{\mathbf{n}}_{\text{OAR}}^{[0]} \right)$  as follows. By updating the LEDs set  $\mathcal{M}$ ,  $\Gamma_i \left( \tilde{\mathbf{n}}_{\text{OAR}}^{[0]} \right)$  is derived by the following the principle: if  $\frac{\mathbf{d}_i^T \tilde{\mathbf{n}}_{\text{OAR}}^{[0]}}{d_i} < \cos(\psi_{\text{FOV}})$ ,  $\Gamma_i \left( \tilde{\mathbf{n}}_{\text{OAR}}^{[0]} \right) = 0$ ; otherwise,  $\Gamma_i \left( \tilde{\mathbf{n}}_{\text{OAR}}^{[0]} \right) = 1$ .

Thus, the proposed PD orientation optimization and projection method is summarized in Algorithm 1.

---

**Algorithm 1** Searching PD orientation

---

- 1: **Initialize:**  $m = 0$ , a feasible beamforming vector  $\mathbf{p}_0$ ;
  - 2: **while**  $\frac{\mathbf{d}_j^T \tilde{\mathbf{n}}_{\text{OAR}}^{[m]}}{d_j} < \cos(\psi_{\text{FOV}})$  **do**
  - 3:     Calculating the problem (31) by using  $\tilde{\mathbf{n}}_{\text{OAR}}^{[m]}$  and update set  $\mathcal{M}$  ;
  - 4:      $m \leftarrow m + 1$ ;
  - 5: **end while**
  - 6: Obtain  $\tilde{\mathbf{n}}_{\text{OAR}}^* \leftarrow \tilde{\mathbf{n}}_{\text{OAR}}^{[m]}$ .
- 

*C. AO algorithm for fixed UE orientation*

In the previous section, we have optimized the beamforming  $\mathbf{P}_0$  and PD orientation vector  $\mathbf{n}_{\text{OAR}}$ . Then, we present the specific alternating optimization algorithm to find the above vector in Algorithm 2. Specifically, we initialize a given receiving orientation vector  $\mathbf{n}_{\text{OAR}}^{[0]}$ , and obtain a beamforming  $\mathbf{P}^{[1]}$  by using the SDR technique. Then, by applying Algorithm 1, we update  $\mathbf{n}_{\text{OAR}}^{[1]}$ . By iteratively calculating  $\mathbf{n}_{\text{OAR}}^{[k]}$  and  $\mathbf{P}^{[k]}$ , the proposed Algorithm 2 will proceed until convergence. The details of algorithm are described as follows.

---

**Algorithm 2** AO Algorithm for Problem (22)

---

- 1: **Initialize:** the convergence criterion  $\delta > 0$ , iteration number  $k = 1$ ;
  - 2: Choose an orientation vector  $\mathbf{n}_{\text{OAR}}^{[0]}$  satisfying  $\sum_{i=1}^N g_i \left( \mathbf{n}_{\text{OAR}}^{[0]} \right) \geq \sqrt{\frac{(2^{\bar{R}/B} - 1) 2\pi B \sigma^2}{e^{(1+2(\alpha_0 + \gamma_0 \varepsilon_0))}} \frac{A}{I_{\text{DC}}}}$ ;
  - 3: Calculating  $\mathbf{P}^{[k]}$  based on (25);
  - 4: Calculating  $\mathbf{n}_{\text{OAR}}^{[k]}$  based on Algorithm 1;
  - 5: **while**  $\left\| \mathbf{n}_{\text{OAR}}^{[k]} - \mathbf{n}_{\text{OAR}}^{[k-1]} \right\| \geq \delta$  **do**
  - 6:      $k \leftarrow k + 1$ ;
  - 7:     Go back to Step 3;
  - 8: **end while**
  - 9: Obtain  $\mathbf{P}^* \leftarrow \mathbf{P}^{[k]}$ ,  $\mathbf{n}_{\text{OAR}}^* \leftarrow \mathbf{n}_{\text{OAR}}^{[k]}$ .
- 

Ultimately, the above AO algorithm is developed to handle problem (19), which includes two key steps, i.e., solving the beamforming design subproblem in Step 3 and the PD orientation optimization subproblem in Step 4. For obtaining beamforming vector  $\mathbf{P}^{[1]}$  and PD orientation vector  $\mathbf{n}_{\text{OAR}}^{[0]}$ , we employ the interior-point algorithm. In conclusion, the total computational complexity of the proposed AO algorithm is approximately  $\mathcal{O} \left( \max \{N + 2, 4\}^4 (N + 3)^{1/2} \log(1/\zeta_2) \right)$ , where  $\zeta_2 > 0$  is the solution accuracy [29].

#### IV. ROBUST JOINT BO OPTIMIZATION FOR RANDOM UE ORIENTATION

In this section, we further investigate robust joint BO scheme for the case of random UE orientation, where the orientation  $\mathbf{n}_{\text{UE}}$  can be random within a certain range.

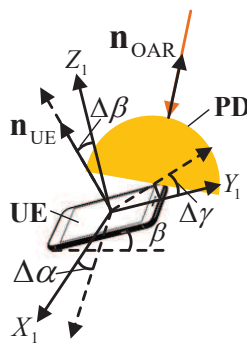


Fig. 4: The random UE orientation model.

Considering the random UE orientation scenario, as shown in Fig. 4, where the UE rotation direction is bounded during information transmission. Specifically, let  $\Delta\alpha \in [-\bar{\alpha}, \bar{\alpha}]$ ,  $\Delta\beta \in [-\bar{\beta}, \bar{\beta}]$ , and  $\Delta\gamma \in [-\bar{\gamma}, \bar{\gamma}]$  denote random angles, where  $\bar{\alpha}$ ,  $\bar{\beta}$  and  $\bar{\gamma}$  denote the corresponding

ranges of the random angles. Then, let  $\mathbf{R}_\Delta = \mathbf{R}_{\Delta\alpha}\mathbf{R}_{\Delta\beta}\mathbf{R}_{\Delta\gamma}$  denote the corresponding UE rotated matrices, where

$$\mathbf{R}_{\Delta\alpha} = \begin{bmatrix} \cos \Delta\alpha & -\sin \Delta\alpha & 0 \\ \sin \Delta\alpha & \cos \Delta\alpha & 0 \\ 0 & 0 & 1 \end{bmatrix}, \mathbf{R}_{\Delta\beta} = \begin{bmatrix} 1 & 0 & 0 \\ 0 & \cos \Delta\beta & -\sin \Delta\beta \\ 0 & \sin \Delta\beta & \cos \Delta\beta \end{bmatrix}, \mathbf{R}_{\Delta\gamma} = \begin{bmatrix} \cos \Delta\gamma & 0 & \sin \Delta\gamma \\ 0 & 1 & 0 \\ -\sin \Delta\gamma & 0 & \cos \Delta\gamma \end{bmatrix}, \quad (32)$$

where  $\Delta\alpha \in [-\bar{\alpha}, \bar{\alpha})$  is the UE yaw random angle, while  $\Delta\beta \in [-\bar{\beta}, \bar{\beta})$  and  $\Delta\gamma \in [-\bar{\gamma}, \bar{\gamma})$  are the UE pitch and roll random angles, respectively.

Based on the above definition, the PD channel gain can be expressed as

$$g_i(\mathbf{n}_{\text{OAR}}) = \lambda_i(\mathbf{x}_{L,i} - \mathbf{r}_{\text{UE}})^T (\mathbf{R}_\Delta^{-1} \mathbf{R}^{-1})^T \mathbf{n}_{\text{OAR}} \Gamma_i(\mathbf{n}_{\text{OAR}}). \quad (33)$$

According to the generalized Lambertian emission model (12), the channel gain  $g_i$  is bounded due to the bounded  $\Delta\alpha, \Delta\beta, \Delta\gamma$ . Specifically, let  $\underline{g}_i(\mathbf{n}_{\text{OAR}})$  and  $\bar{g}_i(\mathbf{n}_{\text{OAR}})$  denote the upper bound and lower bound of  $g_i(\mathbf{n}_{\text{OAR}})$ , i.e.,

$$\underline{g}_i(\mathbf{n}_{\text{OAR}}) \leq g_i(\mathbf{n}_{\text{OAR}}) \leq \bar{g}_i(\mathbf{n}_{\text{OAR}}), \quad (34a)$$

$$\underline{g}_i(\mathbf{n}_{\text{OAR}}) = \underline{\mathbf{q}}_i^T \mathbf{n}_{\text{OAR}} \Gamma_i(\mathbf{n}_{\text{OAR}}), \quad (34b)$$

$$\bar{g}_i(\mathbf{n}_{\text{OAR}}) = \bar{\mathbf{q}}_i^T \mathbf{n}_{\text{OAR}} \Gamma_i(\mathbf{n}_{\text{OAR}}), \quad (34c)$$

where  $\underline{\mathbf{q}}_i = \lambda_i(\mathbf{x}_{L,i} - \mathbf{r}_{\text{UE}})(\mathbf{R}_-^{-1} \mathbf{R}^{-1})$ ,  $\bar{\mathbf{q}}_i = \lambda_i(\mathbf{x}_{L,i} - \mathbf{r}_{\text{UE}})(\mathbf{R}_+^{-1} \mathbf{R}^{-1})$ , and  $\mathbf{R}_-$  and  $\mathbf{R}_+$  are the corresponding rotation matrices to achieve the minimum and maximum of  $g_i(\mathbf{n}_{\text{OAR}})$ , respectively. Thus, the channel gain  $g_i(\mathbf{n}_{\text{OAR}})$  can be re-expressed as

$$g_i(\mathbf{n}_{\text{OAR}}) = \hat{g}_i(\mathbf{n}_{\text{OAR}}) + \Delta g_i, \quad (35)$$

where  $\hat{g}_i(\mathbf{n}_{\text{OAR}})$  denotes the estimated CSI, i.e.,

$$\hat{g}_i(\mathbf{n}_{\text{OAR}}) = \frac{\bar{g}_i(\mathbf{n}_{\text{OAR}}) + \underline{g}_i(\mathbf{n}_{\text{OAR}})}{2} = \frac{(\underline{\mathbf{q}}_i + \bar{\mathbf{q}}_i)^T}{2} \mathbf{n}_{\text{OAR}} \Gamma_i(\mathbf{n}_{\text{OAR}}), \quad (36)$$

and  $\Delta g_i$  denotes the random CSI uncertainty, i.e.,  $|\Delta g_i| \leq \frac{\bar{g}_i(\mathbf{n}_{\text{OAR}}) - \underline{g}_i(\mathbf{n}_{\text{OAR}})}{2}$ .

Let  $\mathbf{g}(\mathbf{n}_{\text{OAR}}) = [g_1(\mathbf{n}_{\text{OAR}}), \dots, g_N(\mathbf{n}_{\text{OAR}})]^T$  denote the channel gain vector between the LEDs

and UE, i.e.,

$$\mathbf{g}(\mathbf{n}_{\text{OAR}}) = \widehat{\mathbf{g}}(\mathbf{n}_{\text{OAR}}) + \Delta\mathbf{g}, \quad (37)$$

where  $\widehat{\mathbf{g}}(\mathbf{n}_{\text{OAR}}) = [\widehat{g}_1(\mathbf{n}_{\text{OAR}}), \dots, \widehat{g}_N(\mathbf{n}_{\text{OAR}})]^T$  is the estimated CSI vector, and  $\Delta\mathbf{g} = [\Delta g_1, \dots, \Delta g_N]^T$  is the CSI uncertainty vector, which can be characterized by the following ellipsoidal region

$$\Omega \triangleq \{\Delta\mathbf{g} | \Delta\mathbf{g}^T \mathbf{C} \Delta\mathbf{g} \leq v\}, \quad (38)$$

where  $\mathbf{C} = \mathbf{C}^T \succeq \mathbf{0}$  controls the extension of the ellipsoid, and  $v$  determines the volume of the ellipsoid. The parameters  $\mathbf{C}$  and  $v$  are determined by the UE rotation range.

Consequently, the received signal at the UE is given as

$$y_{\text{mob}} = (\widehat{\mathbf{g}}(\mathbf{n}_{\text{OAR}}) + \Delta\mathbf{g})^T \mathbf{x} + z. \quad (39)$$

Based on (17), the UE achievable rate is given by

$$R_{\text{mob}}(\mathbf{n}_{\text{OAR}}, \mathbf{p}) = B \log_2 \left( 1 + \frac{|\widehat{\mathbf{g}}(\mathbf{n}_{\text{OAR}}) + \Delta\mathbf{g})^T \mathbf{p}|^2 e^{1+2(\alpha_0 + \gamma_0 \varepsilon_0)}}{2\pi B \sigma^2} \right). \quad (40)$$

For the random UE orientation, the total transmit power is minimized by jointly optimizing the orientation vector  $\mathbf{n}_{\text{OAR}}$  and beamforming vector  $\mathbf{p}$ , which can be formulated as

$$\min_{\mathbf{n}_{\text{OAR}}, \mathbf{p}} \varepsilon \|\mathbf{p}\|^2 \quad (41a)$$

$$\text{s.t. } R_{\text{mob}}(\mathbf{n}_{\text{OAR}}, \mathbf{p}) \geq \bar{R}, \quad (41b)$$

$$\|\mathbf{n}_{\text{OAR}}\|^2 \leq 1, \quad (41c)$$

$$\|(\mathbf{e}_1 + \mathbf{e}_2) \odot \mathbf{n}_{\text{OAR}}\|^2 \leq \sin^2 \bar{\theta}, \quad (41d)$$

$$\cos \bar{\theta} \leq \mathbf{n}_{\text{OAR}}^T \mathbf{e}_3 \leq 1, \quad (41e)$$

$$\Delta\mathbf{g} \in \Omega, \quad (41f)$$

$$\sqrt{P_i} A \leq I_{\text{DC}}, \forall i \in \mathcal{N}. \quad (41g)$$

Due to the fact that the orientation vector  $\mathbf{n}_{\text{OAR}}$  and beamforming vector  $\mathbf{p}$  are coupled together, problem (41) is non-convex. To deal with this issue, we exploit the AO technique to optimize  $\mathbf{n}_{\text{OAR}}$  and  $\mathbf{p}$  alternately. Specifically, we first decouple problem (41) into two subprob-

lems, i.e., a robust beamforming subproblem and a PD orientation optimization subproblem.

### A. Robust Beamforming Design Subproblem

With a given orientation vector  $\mathbf{n}_{\text{OAR}}$ , i.e., given estimated channel gain  $\hat{\mathbf{g}}(\mathbf{n}_{\text{OAR}})$ , we first optimize a robust beamformer to minimize the total transmit power. Specifically, the subproblem is given as

$$\min_{\mathbf{p}} \varepsilon \|\mathbf{p}\|^2 \quad (42a)$$

$$\text{s.t. } B \log_2 \left( 1 + \frac{|\hat{\mathbf{g}}(\mathbf{n}_{\text{OAR}}) + \Delta \mathbf{g})^T \mathbf{p}|^2 e^{1+2(\alpha_0 + \gamma_0 \varepsilon_0)}}{2\pi B \sigma^2} \right) \geq \bar{R}, \quad (42b)$$

$$\Delta \mathbf{g} \in \Omega, \quad (42c)$$

$$\sqrt{P_i} A \leq I_{\text{DC}}, \forall i \in \mathcal{N}. \quad (42d)$$

Moreover, by defining  $\mathbf{P} = \mathbf{p}\mathbf{p}^T$ , the constraint (42b) can be rewritten as

$$\Delta \mathbf{g}^T \mathbf{P} \Delta \mathbf{g} + 2\Delta \mathbf{g}^T \mathbf{P} \hat{\mathbf{g}}(\mathbf{n}_{\text{OAR}}) + \hat{\mathbf{g}}(\mathbf{n}_{\text{OAR}})^T \mathbf{P} \hat{\mathbf{g}}(\mathbf{n}_{\text{OAR}}) \geq c_1, \quad (43)$$

where  $c_1 = \left(2^{\frac{\bar{R}}{B}} - 1\right) \frac{2\pi B \sigma^2}{e^{1+2(\alpha_0 + \gamma_0 \varepsilon_0)}}$ .

Due to the bounded constraint  $\Delta \mathbf{g} \in \Omega$ , the number of constraints in (43) is infinite. Then, based on the S-Procedure, we conservatively transform the infinite constraints to finite linear matrix inequality constraints as detailed next.

By using the S-Procedure [31], the constraints in (43) can be converted as

$$\begin{bmatrix} \mathbf{P} + \eta \mathbf{C} & \mathbf{P} \hat{\mathbf{g}}(\mathbf{n}_{\text{OAR}}) \\ \hat{\mathbf{g}}(\mathbf{n}_{\text{OAR}})^T \mathbf{P} & \hat{\mathbf{g}}(\mathbf{n}_{\text{OAR}})^T \mathbf{P} \hat{\mathbf{g}}(\mathbf{n}_{\text{OAR}}) \\ & -c_1 - \eta v \end{bmatrix} \succeq 0. \quad (44)$$

Furthermore, by ignoring the rank-one constraint of  $\mathbf{P}$  due to SDR, we obtain the following conservative approximation problem as follows.

$$\min_{\mathbf{P}, c_2} \varepsilon \text{Tr}(\mathbf{P}) \quad (45a)$$

$$\text{s.t.} \begin{bmatrix} \mathbf{P} + \eta\mathbf{C} & \mathbf{P}\hat{\mathbf{g}}(\mathbf{n}_{\text{OAR}}) \\ \hat{\mathbf{g}}(\mathbf{n}_{\text{OAR}})^T\mathbf{P} & \hat{\mathbf{g}}(\mathbf{n}_{\text{OAR}})^T\mathbf{P}\hat{\mathbf{g}}(\mathbf{n}_{\text{OAR}}) \\ & -c_1 - \eta v \end{bmatrix} \succeq 0, \quad (45b)$$

$$\text{Tr}(\mathbf{P}\mathbf{e}_i\mathbf{e}_i^T) \leq \frac{I_{\text{DC}}^2}{A}, \forall i \in \mathcal{N}, \quad (45c)$$

$$\mathbf{P} \succeq 0. \quad (45d)$$

Therefore, problem (45) can be solved by the interior-point algorithm [27] [28]. It can be calculated that the complexity of problem (45) is  $\mathcal{O}\left((N+2)^4(N+1)^{1/2}\log(1/\zeta_3)\right)$ , where  $\zeta_3 > 0$  is the solution accuracy [29]. When the rank of the optimal solution is one, we can compute the optimal beamforming vectors by eigenvalue decomposition. Otherwise, we can use the Gaussian randomization procedure to generate a high-quality feasible beamformer vector [29].

### B. PD Orientation Optimization Subproblem

In this subsection, we will optimize the orientation vector  $\mathbf{n}_{\text{OAR}}$  when the transmit beamforming vector  $\mathbf{p}$  is fixed. Specifically, the orientation vector  $\mathbf{n}_{\text{OAR}}$  optimization subproblem can be formulated as follows.

$$\min_{\mathbf{n}_{\text{OAR}}} \varepsilon \|\mathbf{p}\|^2 \quad (46a)$$

$$\text{s.t.} \quad B \log_2 \left( 1 + \frac{|\hat{\mathbf{g}}(\mathbf{n}_{\text{OAR}})^T \mathbf{p}|^2 e^{1+2(\alpha_0 + \gamma_0 \varepsilon_0)}}{2\pi B \sigma^2} \right) \geq \bar{R}, \quad (46b)$$

$$\|\mathbf{n}_{\text{OAR}}\|^2 \leq 1, \quad (46c)$$

$$\|(\mathbf{e}_1 + \mathbf{e}_2) \odot \mathbf{n}_{\text{OAR}}\|^2 \leq \sin^2 \bar{\theta}, \quad (46d)$$

$$\cos \bar{\theta} \leq \mathbf{n}_{\text{OAR}}^T \mathbf{e}_3 \leq 1. \quad (46e)$$

With the fixed  $\mathbf{p}$ , the objective function (46a) does not depend on  $\mathbf{n}_{\text{OAR}}$ . However, when the orientation vector  $\mathbf{n}_{\text{OAR}}$  can achieve the maximum  $(\hat{\mathbf{g}}(\mathbf{n}_{\text{OAR}}))^T \mathbf{p}$ , the power of beamforming vector  $\mathbf{p}$  is the minimum. Thus, the orientation optimization subproblem can be reformulated as

$$\max_{\mathbf{n}_{\text{OAR}}} (\hat{\mathbf{g}}(\mathbf{n}_{\text{OAR}}))^T \mathbf{p} \quad (47a)$$

$$\text{s.t. } (\widehat{\mathbf{g}}(\mathbf{n}_{\text{OAR}}))^T \mathbf{p} \geq c_2, \quad (47b)$$

$$(46c), (46d), (46e).$$

By substituting  $\widehat{g}_i(\mathbf{n}_{\text{OAR}}) = \frac{(\mathbf{q}_i + \bar{\mathbf{q}}_i)}{2} \mathbf{n}_{\text{OAR}} \Gamma_i(\mathbf{n}_{\text{OAR}})$  into  $(\widehat{\mathbf{g}}(\mathbf{n}_{\text{OAR}}))^T \mathbf{p}$ , constraint (47b) can be reformulated as

$$\sum_{n=1}^N \sqrt{p_n} \frac{(\mathbf{q}_n + \bar{\mathbf{q}}_n)^T}{2} \mathbf{n}_{\text{OAR}} \Gamma_n(\mathbf{n}_{\text{OAR}}) \geq c_2, \quad (48)$$

$$\text{where } c_2 = \sqrt{\left(2^{\frac{\bar{R}}{B}} - 1\right) \frac{2\pi B\sigma^2}{e^{1+2(\alpha_0 + \gamma_0 \varepsilon_0)}}}.$$

Thus, the objective function (47a) and constraint (47b) with orientation vector  $\mathbf{n}_{\text{OAR}}$  can be reformulated as

$$\max_{\mathbf{n}_{\text{OAR}}} \sum_{n=1}^N \sqrt{p_n} \frac{(\mathbf{q}_n + \bar{\mathbf{q}}_n)^T}{2} \mathbf{n}_{\text{OAR}} \Gamma_n(\mathbf{n}_{\text{OAR}}) \quad (49a)$$

$$\text{s.t. } \sum_{n=1}^N \sqrt{p_n} \frac{(\mathbf{q}_n + \bar{\mathbf{q}}_n)^T}{2} \mathbf{n}_{\text{OAR}} \Gamma_n(\mathbf{n}_{\text{OAR}}) \geq c_2, \quad (49b)$$

$$(46c), (46d), (46e).$$

Due to the integer and indicator function  $\Gamma_n(\mathbf{n}_{\text{OAR}})$  in both objective function (49a) and constraint (49b), problem (49) is a non-linear non-smooth problem, which is hard to address [30]. To overcome the challenging issue, we propose an alternating optimization and projection method to solve problem (49) iteratively. To be more specific, during the  $k$ th iteration, we relax problem (49) as

$$\max_{\mathbf{n}_{\text{OAR}}} \sum_{j \in \mathcal{M}} \sqrt{p_n} \frac{(\mathbf{q}_n + \bar{\mathbf{q}}_n)^T}{2} \mathbf{n}_{\text{OAR}} \quad (50a)$$

$$\text{s.t. } \sum_{j \in \mathcal{M}} \sqrt{p_n} \frac{(\mathbf{q}_n + \bar{\mathbf{q}}_n)^T}{2} \mathbf{n}_{\text{OAR}} \geq c_2, \quad (50b)$$

$$(46c), (46d), (46e),$$

where  $\mathcal{M} \triangleq \left\{ \forall j \in \mathcal{N} \mid \Gamma_j(\tilde{\mathbf{n}}_{\text{OAR}}^{[k]}) \neq 0 \right\}$  denotes the LEDs set. Then, by applying the standard interior-point algorithm [27], problem (50) can be efficiently solved and the solution  $\tilde{\mathbf{n}}_{\text{OAR}}^{[k]}$  can

be obtained. Then, the LED set  $\mathcal{M}$  is updated. Note that the value of the indicator function  $\Gamma_i(\tilde{\mathbf{n}}_{\text{OAR}}^{[0]})$  is derived by following the principle: If  $\frac{\mathbf{d}_i^T \tilde{\mathbf{n}}_{\text{OAR}}^{[0]}}{d_i} < \cos(\psi_{\text{FOV}})$ ,  $\Gamma_i(\tilde{\mathbf{n}}_{\text{OAR}}^{[0]}) = 0$ ; otherwise,  $\Gamma_i(\tilde{\mathbf{n}}_{\text{OAR}}^{[0]}) = 1$ .

### C. AO algorithm for Random UE orientation

The proposed AO algorithm for jointly robust beamforming design and orientation optimization problem is summarized in Algorithm 3. We first initialize a given receiving orientation vector  $\mathbf{n}_{\text{OAR}}^{[0]}$ , and obtain a robust beamforming vector  $\mathbf{P}^{[1]}$  by solving subproblem (45). Then, we update  $\mathbf{n}_{\text{OAR}}^{[1]}$  by solving subproblem (50). By iteratively calculating  $\mathbf{n}_{\text{OAR}}^{[k]}$  and  $\mathbf{P}^{[k]}$ , the proposed Algorithm 3 proceeds until convergence. The details of algorithm are given as follows.

---

#### Algorithm 3 AO Algorithm for Problem (41)

---

- 1: **Initialize:** given the convergence criterion  $\kappa > 0$ , choose an initial orientation vector  $\mathbf{n}_{\text{OAR}}^{[0]}$ , set the random angle errors  $\Delta\alpha, \Delta\beta, \Delta\gamma$ , and set iteration number  $k = 1$ ;
  - 2: Calculating  $\mathbf{P}^{[k]}$  based on (45);
  - 3: Calculating  $\mathbf{n}_{\text{OAR}}^{[k]}$  based on (50);
  - 4: **while**  $\left\| \mathbf{n}_{\text{OAR}}^{[k]} - \mathbf{n}_{\text{OAR}}^{[k-1]} \right\| \geq \kappa$  **do**
  - 5:      $k \leftarrow k + 1$ ;
  - 6:     Go back to Step 2;
  - 7: **end while**
  - 8: Obtain  $\mathbf{P}^* \leftarrow \mathbf{P}^{[k]}$ ,  $\mathbf{n}_{\text{OAR}}^* \leftarrow \mathbf{n}_{\text{OAR}}^{[k]}$ .
- 

This algorithm includes two main methods solving a robust beamforming design subproblem in Step 2 and a PD orientation optimization subproblem in Step 3. To obtain robust beamforming vector  $\mathbf{P}^{[1]}$  and PD orientation vector  $\mathbf{n}_{\text{OAR}}^{[0]}$ , we use the interior-point algorithm. In conclusion, the total computational complexity of the proposed AO algorithm is approximately  $\mathcal{O}\left(\max\{N+2, 4\}^4(N+3)^{1/2} \log(1/\zeta_4)\right)$ , where  $\zeta_4 > 0$  is the solution accuracy [29].

## V. SIMULATION RESULTS AND DISCUSSIONS

In this section, simulation results are presented to demonstrate the effectiveness of our proposed BO optimization strategies. Consider a VLC system in a room with size of  $(6 \times 6 \times 3) \text{ m}^3$ , and one corner of the room is modeled as the origin  $(0, 0, 0)$  of the Cartesian coordinate system  $(X, Y, Z)$ . The person moves from  $(0, 0)$  to  $(6, 6)$  along the diagonal line of the room. The VLC transmitter contains 9 LEDs, and locations of LEDs are listed in Fig. 5. Moreover, the basic

parameters of the VLC system are listed in Table II. Note that in the case of non-OAR, we only solve the beamforming design problem without optimizing the PD orientation vector  $\mathbf{n}_{\text{OAR}}$ , i.e., the PD orientation  $\mathbf{n}_{\text{OAR}}$  is fixed as  $[0, 0, 1]^T$  in the UE coordinate system.

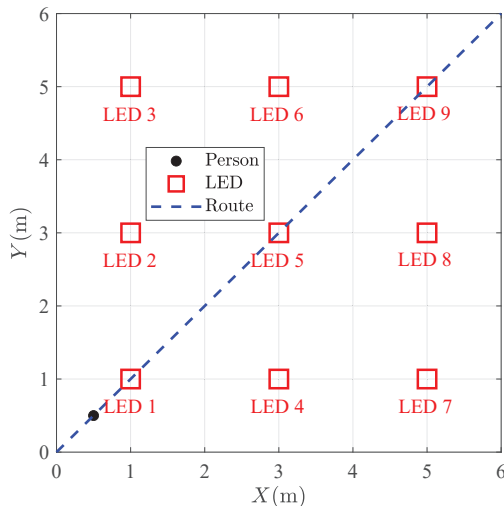


Fig. 5: The schematic of LEDs and User location.

TABLE II: Basic parameters

Definition	Value
Room dimensions ( $W \times L \times H$ )	$(6 \times 6 \times 3) \text{ m}^3$
FoV $\psi_{\text{FOV}}$	$60^\circ$
Detector area of PD $A_{\text{PD}}$	$1 \text{ cm}^2$
Bandwidth $B$	per unit bandwidth*
Average electrical noise power $\sigma^2$	$-98.82 \text{ dBm}$
Half power angle $\phi_{1/2}$	$60^\circ$
DC biasing $I_{\text{DC}}$	$1 \text{ A}$

\* Generally, the bandwidth of VLC system ranges from 10 MHz to 600 MHz [6], [32].

#### A. Performance of OAR System of Fixed UE Orientation

Fig. 6 depicts the LOS, NLOS and blocked regions of the proposed VLC system. In this scenario, a single LED is placed at the  $(3, 3)$  coordinate of the room, and the user's orientation is depicted in Fig. 6. We observe that the green area at the top right corner shows the region blocked by human body. The purple area depicts the LOS region for non-OAR UE. The LOS region for the OAR UE is jointly described by the purple and blue areas. The blue area depicts

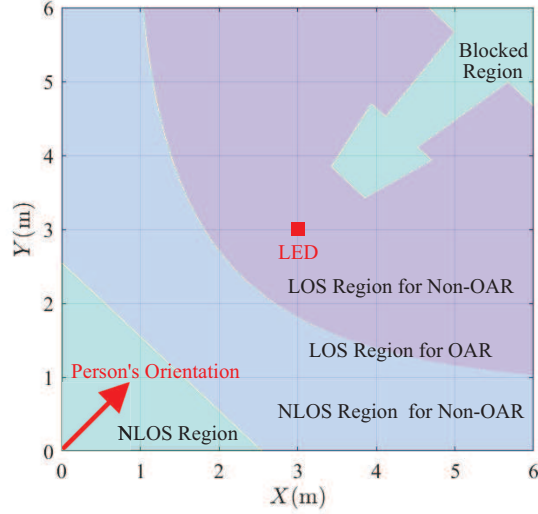


Fig. 6: The schematic of the LOS, NLOS and blocked regions.

the NLOS region of the UE equipped with non-OAR. Moreover, the green area at the left bottom shows the NLOS region for both OAR and non-OAR UE.

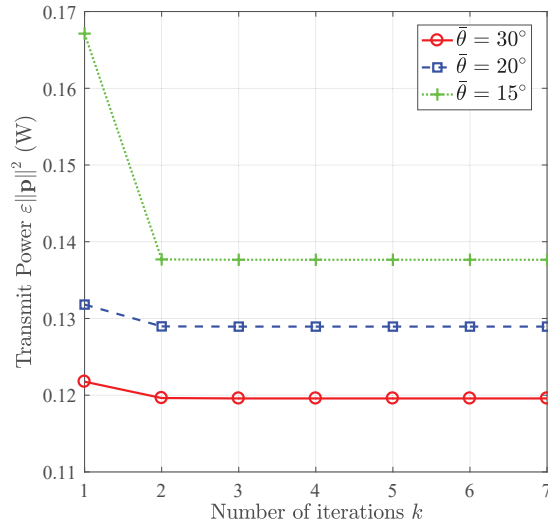


Fig. 7: Transmit power  $\varepsilon\|\mathbf{p}\|^2$  versus the number of iterations  $k$ , with minimum rate threshold  $\bar{R} = 5$  (bits/sec/Hz).

Fig. 7 plots the transmit power  $\varepsilon\|\mathbf{p}\|^2$  versus the number of iterations  $k$  for Algorithm 2 with minimum rate threshold  $\bar{R} = 5$  (bits/sec/Hz). It can be observed that the proposed Algorithm 2 converges within three or four iterations, which demonstrates its effectiveness. Moreover, the total transmit power  $\varepsilon\|\mathbf{p}\|^2$  decreases with the increase of the elevation angle threshold  $\bar{\theta}$ . This is due to the fact that the elevation angle with higher threshold has more degrees of freedom

and can better capture the transmit light signal. Thus, less transmit power is required when the UE is equipped with OAR.

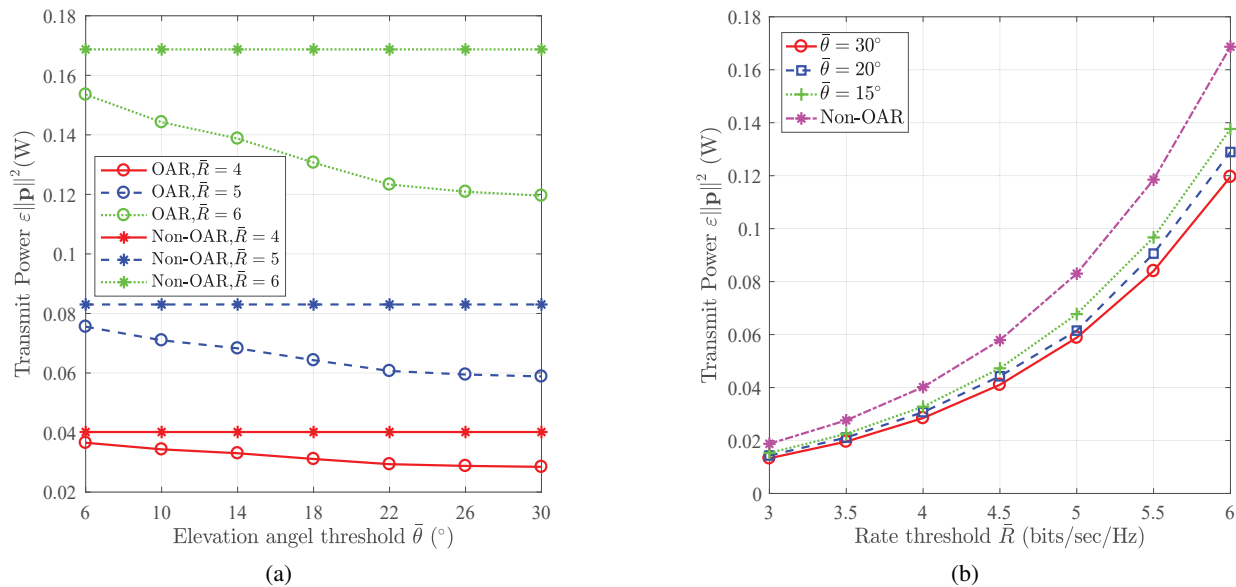


Fig. 8: (a) Transmit power  $\varepsilon \|\mathbf{p}\|^2$  versus the theta threshold with different rate threshold  $\bar{R}$ ; (b) Transmit power  $\varepsilon \|\mathbf{p}\|^2$  versus rate threshold with different elevation angle threshold  $\bar{\theta}$ .

Fig. 8 (a) illustrates the transmit power  $\varepsilon \|\mathbf{p}\|^2$  versus elevation angle threshold with different minimum rate requirements  $\bar{R} = 4$  (bits/sec/Hz), 5 (bits/sec/Hz) and 6 (bits/sec/Hz). It can be observed that the transmit power  $\varepsilon \|\mathbf{p}\|^2$  decreases as the elevation angle threshold increases, for the OAR case, which is same as the result shown in Fig. 7. For the case without OAR, the transmit power is constant as the elevation angle threshold  $\bar{\theta}$  increases. Moreover, comparing with the non-OAR scheme, the total transmit power  $\varepsilon \|\mathbf{p}\|^2$  with OAR is lower. This is because OAR can provide more channel gain. Fig. 8 (b) plots the transmit power  $\varepsilon \|\mathbf{p}\|^2$  versus minimum rate requirement  $\bar{R}$  with different elevation angle thresholds  $\bar{\theta} = 15^\circ$ ,  $20^\circ$  and  $30^\circ$ . We observe that the transmit power  $\varepsilon \|\mathbf{p}\|^2$  increases with rate threshold  $\bar{R}$ . In addition, it can be observed that for the case of OAR, transmit power  $\varepsilon \|\mathbf{p}\|^2$  of the threshold  $\bar{\theta} = 30^\circ$  is lower than the case of  $\bar{\theta} = 20^\circ$ , which is, in turn, lower than that for the case of  $\bar{\theta} = 15^\circ$ . Obviously, the non-OAR scheme consumes more power than the OAR case under the same rate constraint.

Fig. 9 (a) and (b) show the achievable rate  $R$  and transmit power  $\varepsilon \|\mathbf{p}\|^2$  versus the  $X$  coordinate of the user's location, under the minimum rate requirement  $\bar{R} = 1$  (bits/sec/Hz). In Fig. 9 (a), it can be observed that the achievable rate roughly changes periodically with three high points at  $X = 1$  m,  $X = 3$  m and  $X = 5$  m as the  $X$  axis of the user changes from 0 to 6. Meanwhile, the

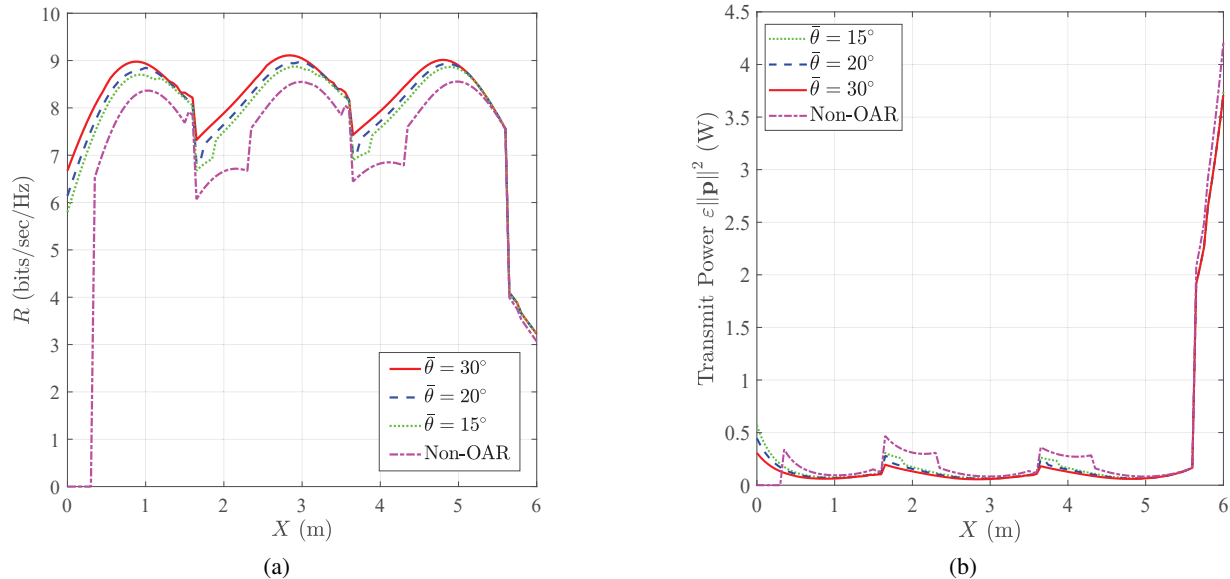


Fig. 9: (a) Achievable rate  $R$  versus the  $X$  coordinate of user's location; (b) Transmit power  $\varepsilon \|\mathbf{p}\|^2$  versus the  $X$  coordinate of user's location with minimum rate threshold  $\bar{R} = 1$  (bits/sec/Hz).

achievable rate  $R$  drops off sharply three times at  $X = 1.65$  m,  $X = 3.65$  m and  $X = 5.65$  m. This is because the signal suffers from human blockage as the user moves away from LED1, LED5 and LED9. We can observe that the achievable rate  $R$  for the case of elevation angle threshold  $\bar{\theta} = 30^\circ$  is higher than that of  $\bar{\theta} = 20^\circ$ , which is, in turn, higher than that of  $\bar{\theta} = 15^\circ$ . Furthermore, the achievable rate  $R$  of OAR with three different elevation angle thresholds is higher than that of the non-OAR scheme. Fig. 9 (b) shows that the transmit power has roughly periodic behavior with three low points at  $X = 1$  m,  $X = 3$  m and  $X = 5$  m as the  $X$  coordinate of the user changes from 0 to 6. Meanwhile, the transmit power  $\varepsilon \|\mathbf{p}\|^2$  increases sharply three times at  $X = 1.65$  m,  $X = 3.65$  m and  $X = 5.65$  m. This is again due to signal suffering from human blockage. Other conclusions from this figure are the same as those of Fig. 9 (a).

### B. Performance of OAR system for Random UE Orientation

In the following, we compare the proposed robust joint BO design scheme with the non-robust joint BO design scheme, which does not handle random UE orientation, and the perfect joint BO design scheme, where the random angle errors  $\Delta\alpha$ ,  $\Delta\beta$  and  $\Delta\gamma$  are zero.

Fig. 10 shows the cumulative distribution function (CDF) of the achievable rate, where the elevation angle threshold  $\bar{\theta} = 30^\circ$ , the minimum rate threshold  $\bar{R} = 5$  (bits/sec/Hz) and random angle errors  $\Delta\alpha \in [-0.5^\circ, 0.5^\circ]$ ,  $\Delta\beta \in [-0.5^\circ, 0.5^\circ]$ ,  $\Delta\gamma \in [-0.5^\circ, 0.5^\circ]$ , respectively. The

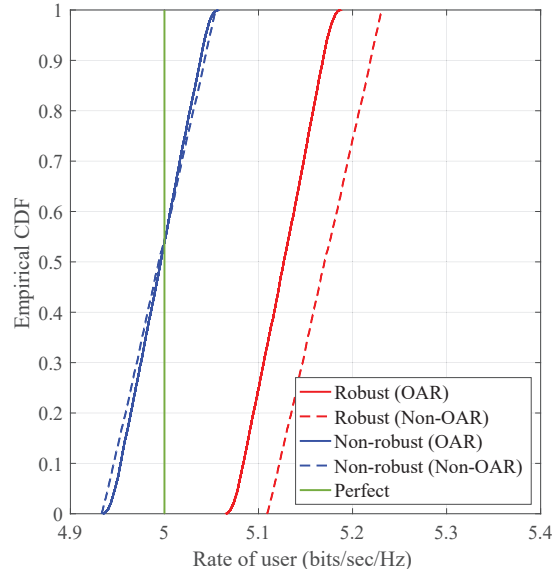
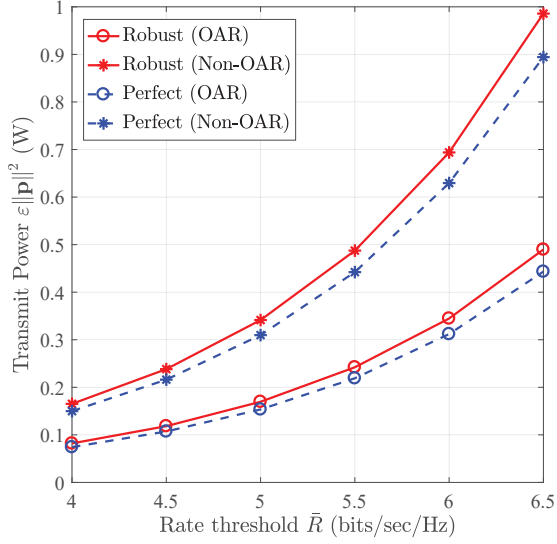


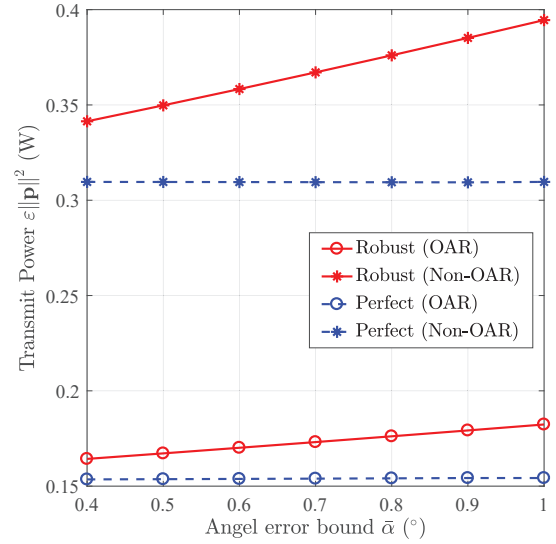
Fig. 10: The empirical CDF of rate, with elevation angle threshold  $\bar{\theta} = 30^\circ$ , minimum rate threshold  $\bar{R} = 5$  (bits/sec/Hz) and random angle errors  $\Delta\alpha \in [-0.5^\circ, 0.5^\circ)$ ,  $\Delta\beta \in [-0.5^\circ, 0.5^\circ)$ ,  $\Delta\gamma \in [-0.5^\circ, 0.5^\circ)$ .

CDF of rate is over 10000 random channel realizations by Monte-Carlo simulation. On one hand, both the robust design with OAR and non-OAR satisfy the minimum rate requirement. On the other hand, the non-robust with OAR and non-OAR schemes cannot always guarantee the minimum rate constraint. It can also be verified that the proposed robust design with OAR is less conservative than the robust design with non-OAR.

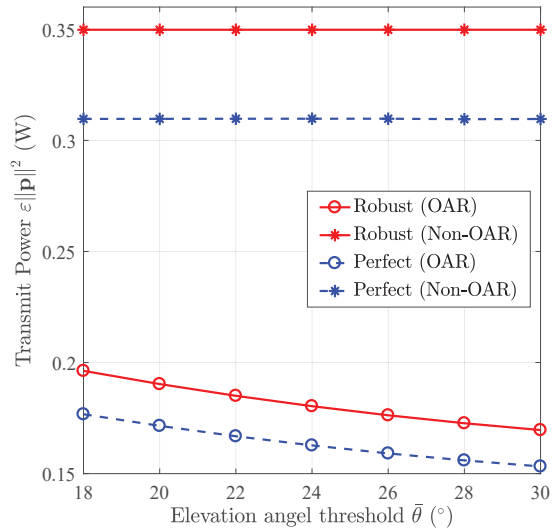
Fig. 11 (a) shows the transmit power  $\varepsilon\|\mathbf{p}\|^2$  versus minimum rate threshold  $\bar{R}$ , in the case of elevation angle threshold  $\bar{\theta} = 30^\circ$  and random angle errors  $\Delta\alpha \in [-0.5^\circ, 0.5^\circ)$ ,  $\Delta\beta \in [-0.5^\circ, 0.5^\circ)$ ,  $\Delta\gamma \in [-0.5^\circ, 0.5^\circ)$ . We can observe that the transmit power of the all aforementioned BO optimization schemes increases with minimum rate threshold. Moreover, the transmit power of the robust beamforming design is less than that of the robust design with non-OAR. Fig. 11 (b) illustrates the transmit power  $\varepsilon\|\mathbf{p}\|^2$  versus random angle error bound  $\bar{\alpha}$ , with minimum rate threshold  $\bar{R} = 5$  (bits/sec/Hz) and elevation angle threshold  $\bar{\theta} = 30^\circ$ . We observe that as the random angle error bound  $\bar{\alpha}$  increases, the transmit power of the robust beamforming design for both OAR and non-OAR increases, where the transmit power of the OAR robust beamforming design is less than the robust design with the non-OAR. However, both perfect cases are constant when the random angle error increases. This is because a large random angle error may lead to a bad beamformer design, which leads to increasing the transmit power  $\varepsilon\|\mathbf{p}\|^2$ . Fig. 11 (c) shows the transmit power  $\varepsilon\|\mathbf{p}\|^2$  versus elevation angle threshold  $\bar{\theta}$ ,



(a)



(b)



(c)

Fig. 11: (a) Transmit power  $\epsilon \|\mathbf{p}\|^2$  versus minimum rate threshold  $\bar{R}$ ; (b) Transmit power  $\epsilon \|\mathbf{p}\|^2$  versus random angle error bound  $\bar{\alpha}$ ; (c) Transmit power  $\epsilon \|\mathbf{p}\|^2$  versus elevation angle threshold  $\bar{\theta}$ .

with minimum rate threshold  $\bar{R} = 5$  (bits/sec/Hz) and random angle errors  $\Delta\alpha \in [-0.5^\circ, 0.5^\circ)$ ,  $\Delta\beta \in [-0.5^\circ, 0.5^\circ)$ ,  $\Delta\gamma \in [-0.5^\circ, 0.5^\circ)$ . We observe that as elevation angle threshold  $\bar{\theta}$  increases, the transmit power of OAR UE decreases for both robust and perfect scenarios. This is because OAR UE can provide more channel gains, which leads to less transmit power.

## VI. CONCLUSIONS

In this paper, we investigate the joint BO schemes by considering the assistance of an adjustable orientation receiver with fixed and random UE orientation. For the fixed UE orientation, the joint BO optimization problem is nonconvex and coupled. We develop an alternating optimization algorithm to optimize the transmit beamforming and PD orientation vectors. For the random UE orientation, we further propose a robust alternating optimization algorithm based on the S-lemma. Finally, the performance of the joint BO optimization designs are evaluated through numerical experiments. Our examinations show that proposed joint BO schemes enhance the QoS of the UE with less transmit power consumption compared to benchmark schemes.

## REFERENCES

- [1] V. W. S. Wong, R. Schober, D. Ng, and L. C. Wang, *Key technologies for 5G wireless systems*, Cambridge, U.K.: Cambridge Univ, 2017.
- [2] L. Chettri and R. Bera, "A comprehensive survey on internet of things (IoT) toward 5G wireless systems," *IEEE Internet Things J.*, vol. 7, no. 1, pp. 16–32, Jan. 2020.
- [3] M. Agiwal, A. Roy, and N. Saxena, "Next generation 5G wireless networks: A comprehensive survey," *IEEE Commun. Surveys Tuts.*, vol. 18, no. 3, pp. 1617–1655, Jul.-Sep. 2016.
- [4] A. M. Abdelhady, O. Amin, A. Chaaban, B. Shihada, and M.-S. Alouini, "Spectral-efficiency-illumination pareto front for energy harvesting enabled VLC systems," *IEEE Trans. Commun.*, vol. 67, no. 12, pp. 8557–8572, Dec. 2019.
- [5] T. Tang, T. Shang, and Q. Li, "Impact of multiple shadows on visible light communication channel," *IEEE Commun. Lett.*, vol. 25, no. 2, pp. 513–517, Feb. 2021.
- [6] P. H. Pathak, X. Feng, P. Hu, and P. Mohapatra, "Visible light communication, networking, and sensing: A survey, potential and challenges," *IEEE Commun. Surveys Tuts.*, vol. 17, no. 4, pp. 2047–2077, Sep. 2015.
- [7] A. Nuwanpriya, S.-W. Ho, and C. S. Chen, "Indoor MIMO visible light communications: Novel angle diversity receivers for mobile users," *IEEE J. Sel. Areas Commun.*, vol. 33, no. 9, pp. 1780–1792, Sep. 2015.
- [8] C. Chen, W.-D. Zhong, H. Yang, S. Zhang, and P. Du, "Reduction of SINR fluctuation in indoor multi-cell VLC systems using optimized angle diversity receiver," *IEEE/OSA J. Lightw. Technol.*, vol. 36, no. 17, pp. 3603–3610, Sep. 2018.
- [9] O. Z. Alsulami, K. D. Alazwary, S. O. M. Saeed, S. H. Mohamed, T. E. H. El-Gorashi, M. T. Alresheedi, and J. M. H. Elmirghani, "Effect of receiver orientation on resource allocation in optical wireless systems," in *2020 22nd International Conference on Transparent Optical Networks (ICTON)*, pp. 1–6, 2020.
- [10] Y. S. Eroglu, C. K. Anjinappa, A. Guvenc, and N. Pala, "Slow beam steering and NOMA for indoor multi-user visible light communications," *IEEE Trans. Mob. Comput.*, vol. 20, no. 4, pp. 1627–1641, Apr. 2021.
- [11] I. Abdalla, M. Rahaim, and T. Little, "Impact of receiver FOV and orientation on dense optical networks," in *Proc. IEEE Global Commun. Conf. (GLOBECOM)*, pp. 1–6, 2018.
- [12] I. Abdalla, M. B. Rahaim, and T. D. C. Little, "Dynamic fov visible light communications receiver for dense optical networks," *IET Commun.*, vol. 13, no. 7, pp. 822–830, Feb. 2019.
- [13] I. Abdalla, M. B. Rahaim, and T. D. C. Little, "Interference mitigation through user association and receiver field of view optimization in a multi-user indoor hybrid RF/VLC illuminance-constrained network," *IEEE Access*, vol. 8, pp. 228779–228797, Dec. 2020.

- [14] M. Morales-Céspedes, H. Haas, and A. G. Armada, "Optimization of the receiving orientation angle for zero-forcing precoding in VLC," *IEEE Commun. Lett.*, vol. 25, no. 3, pp. 921–925, Mar. 2021.
- [15] A. She, S. Zhang, S. Shian, D. R. Clarke, and F. Capasso, "Adaptive metalenses with simultaneous electrical control of focal length, astigmatism, and shift," *Sci. Adv.*, vol. 4, no. 2, pp. eaap9957, 2018.
- [16] Q. Fan, D. Wang, P. Huo, Z. Zhang, and T. Xu, "Autofocusing airy beams generated by all-dielectric metasurface for visible light," *Opt. Express*, vol. 25, no. 8, pp. 9285–9294, Apr. 2017.
- [17] S. M. Kamali, E. Arbabi, A. Arbabi, and A. Faraon, "A review of dielectric optical metasurfaces for wavefront control," *Nanophotonics*, vol. 7, no. 6, pp. 1041–1068, May. 2018.
- [18] J. Notaros, M. Notaros, M. Raval, and M. R. Watts, "Liquid-crystal-based visible-light integrated optical phased arrays," in *2019 Conference on Lasers and Electro-Optics (CLEO)*, pp. 1–2, 2019.
- [19] A. R. Ndjiongue, T. M. N. Ngatched, O. A. Dobre, and H. Haas, "Toward the use of re-configurable intelligent surfaces in VLC systems: Beam steering," *IEEE Wireless Commun.*, vol. 28, no. 3, pp. 156–162, Jul. 2021.
- [20] A. R. Ndjiongue, T. M. N. Ngatched, O. A. Dobre, and H. Haas, "Re-configurable intelligent surface-based VLC receivers using tunable liquid-crystals: The concept," *IEEE/OSA J. Lightw. Technol.*, vol. 39, no. 10, pp. 3193–3200, May. 2021.
- [21] Y. A. S. T. Q. Wang and J. Armstrong, "Analysis of an optical wireless receiver using a hemispherical lens with application in MIMO visible light communications," *IEEE/OSA J. Lightw. Technol.*, vol. 31, no. 11, pp. 1744–1754, Jun. 2013.
- [22] T. Fath and H. Haas, "Performance comparison of MIMO techniques for optical wireless communications in indoor environments," *IEEE Trans. Commun.*, vol. 61, no. 2, pp. 733–742, Feb. 2013.
- [23] Z. Zeng, M. D. Soltani, H. Haas, and M. Safari, "Orientation model of mobile device for indoor VLC and millimetre wave systems," in *Proc. IEEE 88th Veh. Technol. Conf. (VTC Fall)*, Chicago, IL, USA, pp. 1–6, 2018.
- [24] M. Sun, X. Xu, X. W. Sun, X. Liang, V. Valuckas, Y. Zheng, R. Paniagua-Domínguez, and A. I. Kuznetsov, "Efficient visible light modulation based on electrically tunable all dielectric metasurfaces embedded in thin-layer nematic liquid crystals," *Sci. Rep.*, 2019.
- [25] S. Aboagye, T. M. N. Ngatched, O. A. Dobre, and A. R. Ndjiongue, "Intelligent reflecting surface-aided indoor visible light communication systems," *IEEE Commun. Lett.*, vol. 25, no. 12, pp. 3913–3917, Dec. 2021.
- [26] S. Ma, R. Yang, H. Li, Z.-L. Dong, H. Gu, and S. Li, "Achievable rate with closed-form for siso channel and broadcast channel in visible light communication networks," *IEEE/OSA J. Lightw. Technol.*, vol. 35, no. 14, pp. 2778–2787, Jul. 2017.
- [27] J. F. Sturm, "Using SeDuMi 1.02, a Matlab toolbox for optimization over symmetric cones," *Optimization Methods and Software*, vol. 11, no. 1-4, pp. 625–653, 1999.
- [28] M. Grant and S. Boyd, "CVX: Matlab software for disciplined convex programming," <http://stanford.edu/boyd/cvx>, Jun. 2009.
- [29] Z. quan Luo, W. kin Ma, A. So, Y. Ye, and S. Zhang, "Semidefinite relaxation of quadratic optimization problems," *IEEE Signal Process. Mag.*, vol. 27, no. 3, pp. 20–34, May 2010.
- [30] D. Luenberger, *Linear and Nonlinear Programming*, Stanford University, California, 1984.
- [31] S. Boyd and L. Vandenberghe, *Convex Optimization*, Cambridge University Press, 2004.
- [32] S. Ma, F. Zhang, H. Li, F. Zhou, M.-S. Alouini, and S. Li, "Aggregated VLC-RF systems: Achievable rates, optimal power allocation, and energy efficiency," *IEEE Trans. Wireless Commun.*, vol. 19, no. 11, pp. 7265–7278, Nov. 2020.